You Only Scan Once: Efficient Multi-dimension Sequential Modeling with LightNet

Anonymous authors
Paper under double-blind review

Abstract

Linear attention mechanisms have gained prominence in causal language models due to their linear computational complexity and enhanced speed. However, the inherent decay mechanism in linear attention presents challenges when applied to multi-dimensional sequence modeling tasks, such as image processing and multi-modal learning. In these scenarios, the utilization of sequential scanning to establish a global receptive field necessitates multiple scans for multi-dimensional data, thereby leading to inefficiencies. This paper identifies the inefficiency caused by a "multiplicative decay" linear recurrence and proposes an efficient alternative "additive decay" linear recurrence to avoid the issue, as it can handle multi-dimensional data within a single scan. We further develop an efficient multi-dimensional sequential modeling framework called LightNet based on the new recurrence. Moreover, we present two new multi-dimensional linear relative positional encoding methods, MD-TPE and MD-LRPE to enhance the model's ability to discern positional information in multi-dimensional scenarios. Our empirical evaluations across various tasks, including image classification, image generation, bidirectional language modeling, and autoregressive language modeling, demonstrate the efficacy of LightNet, showcasing its potential as a versatile and efficient solution for multi-dimensional sequential modeling.

1 Introduction

Linear attention has emerged as an effective alternative to softmax attention due to its linear computational complexity and enhanced processing speed, especially in causal language models (Peng et al., 2024; Qin et al., 2023a). The benefits of linear attention largely depend on its decay mechanism (Peng et al., 2024; Qin et al., 2023a; Sun et al., 2023b), which prevents attention dilution (Qin et al., 2022) and facilitates global interaction among tokens. However, the decay mechanism presents two primary issues: First, the decay mechanism is not easily applicable to high-dimensional inputs due to the need for multiple sequential scans to establish a global multi-dimensional receptive field, which reduces computational efficiency (Duan et al., 2024; Zhu et al., 2024). Additionally, without the decay mechanism, linear attention lacks positional awareness during computations, leading to decreased performance (Qin et al., 2022). In light of these challenges, we are investigating the feasibility of reducing sequential scans for multi-dimensional scenarios while preserving performance.

We first analyze the types of linear recurrence and divide them into two categories: *multiplicative* and *additive*. In multiplicative recurrence, the decay rate is dependent only on the current moment, making it impossible to obtain information about subsequent moments with a single scan. By taking image processing as an example, using multiplicative decay recurrence will require at least two scans to retrieve the global information (Duan et al., 2024; Zhu et al., 2024). Conversely, in additive decay recurrence, the decay rate depends on all moments through the summation of the importance score of each moment, enabling it to gather global information in a single scan.

It is important to note that in non-causal situations, additive recurrence is permutation-invariant, which means it lacks local precedence and therefore diminishes the capture of positional information. To overcome this limitation, we put forth a new approach to positional encoding called Multi-Dimensional Toeplitz Posi-

tional Encoding (MD-TPE). This method utilizes the mathematical properties of the Toeplitz matrix to embed relative positional information with linear time complexity, thus ensuring efficiency in multi-dimensional scenarios. Additionally, we expand the Linearized Relative Positional Encoding (LRPE) (Qin et al., 2023b) to high-dimensional scenarios, resulting in the creation of Multi-Dimensional Linearized Relative Positional Encoding (MD-LRPE).

We then present LightNet, a new multi-dimensional linear attention model built on additive decay recurrence. LightNet features a pioneering decay mechanism, allowing for efficient single-scan processing of high-dimensional sequential data. Furthermore, it integrates highly effective multi-dimensional position encoding such as MD-TPE and MD-LRPE to precisely capture positional information.

We conduct several evaluations of the performance of our proposed LightNet on a range of tasks, including image generation, image classification, bidirectional language modeling, and autoregressive language modeling. LightNet performs comparably or better than its competitors across all tasks.

We summarize our main contributions as follows:

- We analyze the types of linear recurrence, dividing them into two types: *multiplicative* and *additive*, where the additive type can obtain global information in a single scan.
- We propose two multi-dimensional position encoding strategies, MD-TPE and MD-LRPE, to effectively capture positional information in multi-dimensional scenarios.
- We propose LightNet, a new multi-dimensional linear attention model that can process high-dimensional sequences in a single scan.
- We conduct thorough evaluations to assess the efficiency and efficacy of LightNet for multi-dimensional sequential modeling tasks. The LightNet demonstrates competitive performance in all scenarios.

2 Related Work

Linear Attention. The linear attention mechanism has greatly advanced deep learning, particularly in natural language processing, by providing a scalable solution for long input sequences and reducing the computational demands of traditional attention models (Choromanski et al., 2020; Katharopoulos et al., 2020; Qin et al., 2021). However, despite its faster training speeds, the performance of linear attention still falls short of softmax attention due to the attention dilution issue (Qin et al., 2022). The TNL/RetNet (Qin et al., 2022; 2023a) introduces a decay mechanism to address this problem. Additionally, GLA (Yang et al., 2023) incorporating gating mechanisms shows the potential to enhance linear attention models.

State Space Model. State Space Models (SSMs) are increasingly crucial in sequence modeling due to their structured approach to capturing temporal dynamics through latent variables. The S4 model (Gu et al., 2021) enhances state space modeling for long sequences by leveraging structured spaces to improve computational efficiency and tackle complex dynamics. With additional parameterizing and initializing diagonal state space strategy (Gu et al., 2022), the SSMs can achieve comparable performance to naive transformers. Furthermore, the Gated State Space (GSS) model (Mehta et al., 2023) introduces a gating mechanism to SSMs, which is particularly effective for long-range language modeling by allowing nuanced control over information flow. The S5 model (Smith et al., 2022) reduces complexity using "scan" while maintaining the capability to handle intricate sequences. However, directly extending the SSM to multi-dimensional input usually requires multiple sequential scans, which will reduce the computational efficiency (Zhu et al., 2024).

Linear RNN. Linear RNNs employ element-wise recursion for sequence modeling, and due to their linear recursive form, they can be accelerated using parallel scans (Martin & Cundy, 2018). At their core is the decay mechanism, where RWKV-4/LRU (Peng et al., 2024; Orvieto et al., 2023) utilizes data-independent decay. HGRN (Qin et al., 2024c;b) leverage data-dependent decay to enhance performance. Linear RNNs have shown considerable potential in language modeling and long-sequence modeling tasks.

Multi-dimensional Tasks with Linear Complexity Model. The development of linear attention in language models has led to its extension into multi-dimensional tasks. Building upon the cosFormer frame-

work (Qin et al., 2021), VVT (Sun et al., 2023a) explores a local prior of 2D linear attention and applies it to image classification tasks. Vim (Zhu et al., 2024) and Vision-RWKV (Duan et al., 2024) utilize a sequential scan mechanism to expand Mamba (Gu & Dao, 2023) and RWKV (Peng et al., 2023) for image classification. Additionally, leveraging the benefits structure of the diffusion transformer (Peebles & Xie, 2023) in image generation, several works have extended linear complexity models into 2D space (Fei et al., 2024a;b; Yan et al., 2023; Hu et al., 2024) to replace the traditional transformer architecture, achieving efficient image generation. However, some of these tasks encounter issues with inadequate performance. Moreover, frequent sequential scans can compromise the efficiency of the model.

3 Preliminary

In this section, we provide preliminary knowledge about softmax attention (Vaswani et al., 2017), linear attention (Katharopoulos et al., 2020), and linear attention with decay (Qin et al., 2021; 2024a).

Softmax attention operates on query $\mathbf{Q}$, key $\mathbf{K}$ and value $\mathbf{V}$ matrices. Each of them is the image of a linear projection taking input $\mathbf{X} \in \mathbb{R}^{n \times d}$ as input:

$$\mathbf{O} = \text{Softmax}(\mathbf{Q}\mathbf{K}^\top / \sqrt{d})\mathbf{V},$$

with n the input length, d the hidden dimension. Computing $\text{Softmax}(\mathbf{Q}\mathbf{K}^\top / \sqrt{d})$ needs $O(n^2)$ time complexity, which makes Softmax attention very costly when processing long documents.

Linear attention removes the softmax function and uses a kernel function $\phi(.)$ (Katharopoulos et al., 2020; Qin et al., 2021; Choromanski et al., 2020) to map queries and keys to hidden representations, the formulation can be written as:

$$\mathbf{O} = \mathbf{\Delta}^{-1}\phi(\mathbf{Q})[\phi(\mathbf{K})^\top \mathbf{V}], \mathbf{\Delta} = \text{diag}(\phi(\mathbf{Q})[\phi(\mathbf{K})^\top \mathbf{1}_n]).$$

Since $\phi(\mathbf{K})^\top \mathbf{V}$ is computed first, the time complexity is $O(n)$. Qin et al. (2022) find the denominator term $\mathbf{\Delta}$ makes the training unstable and replace it with an extra-normalization function, the normalization can be layernorm (Ba et al., 2016), rmsnorm (Zhang & Sennrich, 2019), srmsnorm (Qin et al., 2023a), and the formulation can be simplified as:

$$\mathbf{O} = \text{Norm}\left(\phi(\mathbf{Q})[\phi(\mathbf{K})^\top \mathbf{V}]\right), \tag{1}$$

In a causal scenario, such as in a language model, linear attention can be written in a recursive form (Katharopoulos et al., 2020) (here we ignore normalization and kernel function ϕ):

$$\mathbf{kv}_0 = \mathbf{0}, \mathbf{kv}_t = \mathbf{kv}_{t-1} + \mathbf{k}_t \mathbf{v}_t^\top, \mathbf{o}_t^\top = \mathbf{q}_t^\top \mathbf{kv_t}, t = 1, \ldots, n.$$

Linear attention with decay means that a decay term λ_t in the recursion (Qin et al., 2023a; 2024c;b):

$$\mathbf{kv}_0 = \mathbf{0}, \mathbf{kv}_t = \lambda_t \mathbf{kv}_{t-1} + \mathbf{k}_t \mathbf{v}_t^\top, \mathbf{o}_t^\top = \mathbf{q}_t^\top \mathbf{kv_t}, t = 1, \ldots, n, 0 < \lambda_t \leq 1. \tag{2}$$

When the decay term λ_t is independent of the input (*i.e.*, $\lambda_t = \lambda$), it is also known as data-independent decay (Qin et al., 2023a; Sun et al., 2023b). When the term λ_t is related to the input, it is referred to as data-dependent decay (Yang et al., 2023; Qin et al., 2024c;b; Gu & Dao, 2023). Note that the decay term is essential for enhancing the performance of linear attention. Removing the decay term results in a significant drop in performance. However, the decay term also presents a major challenge when trying to effectively apply linear attention to multidimensional data as the "right product" trick cannot be used in this scenario (Qin et al., 2023a; Yang et al., 2023).

4 Linear Recurrence in Multi-dimensional Space

In this section, we discuss the theoretical and practical computational complexity of linear recurrence (with decay) when dealing with high-dimensional data, and then analyze the types of linear recurrence. In subsequent discussions, we assume n is the sequence length, d is the embedding dimension, and $\mathbf{x}_t \in \mathbb{R}^d$ is the transpose of the t-th row of matrix $\mathbf{X} \in \mathbb{R}^{n \times d}$.

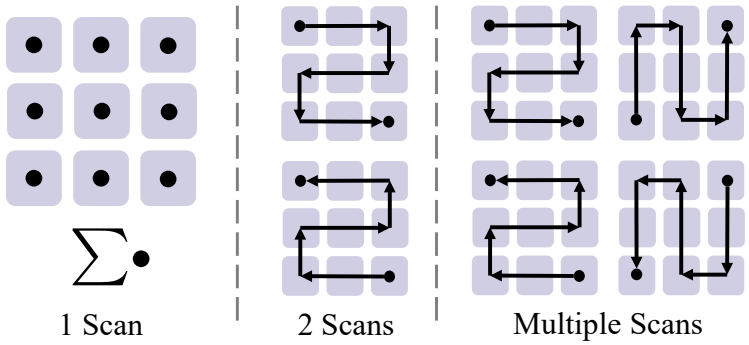

Figure 1: Illustration of different scan numbers. Different from the methods that perform multiple scans, our proposed method only performs "1 scan", which sum all tokens together directly, as shown in the figure on the left.

4.1 Computational Complexity of Linear Recurrence

Eq. 2 illustrates the linear recurrence in causal scenarios. When dealing with non-causal scenarios, a common practice in the literature is to perform causal computation twice (Duan et al., 2024; Zhu et al., 2024). We call this method "2 scan":

$$\overrightarrow{\mathbf{kv}}_0 = \mathbf{0}, \overrightarrow{\mathbf{kv}}_t = \lambda_t \overrightarrow{\mathbf{kv}}_{t-1} + \mathbf{k}_t \mathbf{v}_t^\top, \overrightarrow{\mathbf{o}}_t^\top = \mathbf{q}_t^\top \overrightarrow{\mathbf{kv}}_t,$$
$$\overleftarrow{\mathbf{kv}}_{n+1} = \mathbf{0}, \overleftarrow{\mathbf{kv}}_t = \lambda_t \overleftarrow{\mathbf{kv}}_{t+1} + \mathbf{k}_t \mathbf{v}_t^\top, \overleftarrow{\mathbf{o}}_t^\top = \mathbf{q}_t^\top \overleftarrow{\mathbf{kv}}_t,$$
$$\mathbf{o}_t = \overrightarrow{\mathbf{o}}_t + \overleftarrow{\mathbf{o}}_t.$$

When $\lambda_t = 1$, *i.e.* there is no decay, the right product trick (Katharopoulos et al., 2020) can be applied in this case. We call this method "1 scan", as shown in Fig. 1.

$$[\mathbf{KV}] = \mathbf{K}^\top \mathbf{V}, \mathbf{O} = \mathbf{Q}[\mathbf{KV}].$$

Although both of the above formulas have a time complexity of $O(nd^2)$, the "2 scan" version is significantly slower than the "1 scan" version. This is because causal computation requires block-level recursion (Qin et al., 2024a; Yang et al., 2023), whereas the second formula can be fully parallelized due to matrix multiplication (Katharopoulos et al., 2020). We provide a speed comparison in Fig. 2, where the "2 scan" is implemented with Lightning Attention (Qin et al., 2024a), the fastest linear attention implementation so far. It can be seen that the "2 scan" is several times slower than the "1 scan" in both forward and backward passes.

It is apparent that the need for multiple scans is mainly due to the presence of decay λ_t. However, directly removing λ_t would lead to degraded performance (Qin et al., 2022). A natural question arises: *can we retain λ_t while only performing a single scan?* In the next section, we will discuss the types of linear recurrence and answer the question.

4.2 Types of Linear Recurrence

We first explore the representation range of linear recurrences by 1D linear recurrence, Here, we assume $a_t \triangleq f(x_1, \ldots, x_t)$, $f : \mathbb{R} \to \mathbb{R}$ is some function. It indicates that a_t is data-dependent, i.e., depending on the input tokens.[1]:

$$y_t = a_t y_{t-1} + x_t, y_0 = 0. \tag{3}$$

Unroll the recursion equation of Eq. 3, we obtain:

$$y_t = \sum_{s=1}^{t} \frac{A_s}{A_t} x_s \triangleq \sum_{s=1}^{t} c_{ts} x_s, A_t = \left(\prod_{s=1}^{t} a_s \right)^{-1}. \tag{4}$$

[1]This assumption is commonly adopted in the Linear Attention and RNN communities. (Yang et al., 2023; Gu & Dao, 2023)

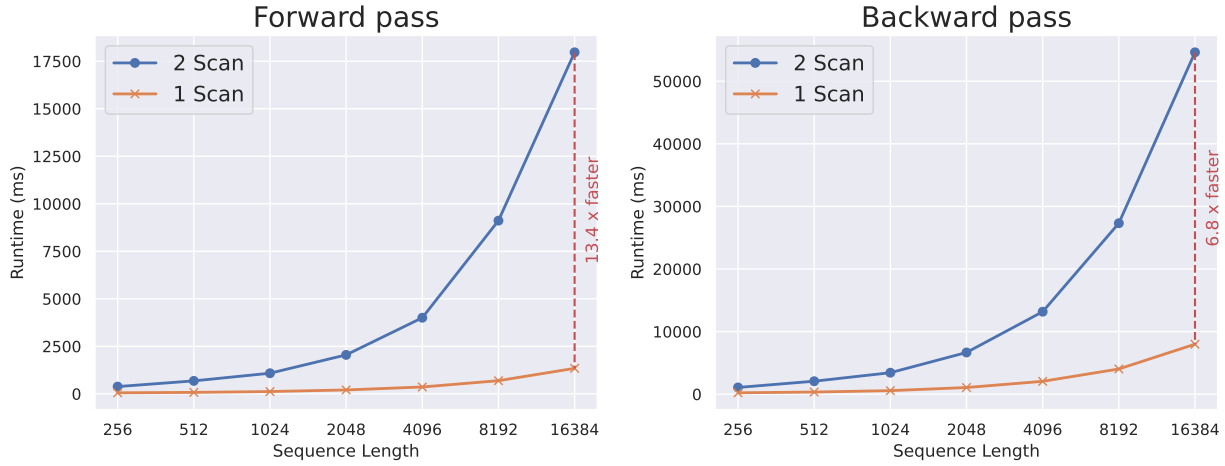

Figure 2: **Processing time of 1 Scan and 2 Scan in relation to sequence length.** 1 Scan is significantly faster than 2 Scan in both forward and backward passes. As the sequence length increases, the advantage of 1 Scan becomes more substantial. Note that the x-axis scale follows a logarithmic scale to enhance visualization clarity.

The detailed proof of the unrolling process can be found in Appendix A.1. Note that y_t is a linear combination of $x_1, \ldots, x_t$. A natural question arises: *Can every linear combination* $\sum_{s=1}^{t} c_{ts} x_s$ *be represented as a linear recursion?* We now prove that a linear recursion representation is possible only when the coefficients c_{ts} satisfy certain conditions.

Theorem 4.1. *A linear recurrence* $y_t = a_t y_{t-1} + x_t, y_0 = 0$ *is equivalent to a linear combination* $y_t = \sum_{s=1}^{t} c_{ts} x_s$, *iff* $c_{ts} = \frac{g_s}{g_t}$, *where* $g_t = g(x_1, \ldots, x_t)$.

Proof of Theorem 4.1. $\Rightarrow$

Given a linear recurrence, we multiply it by $A_t = \left(\prod_{s=1}^{t} a_s\right)^{-1}$ and following recurrence equation:

$$A_t y_t = A_t a_t y_{t-1} + A_t x_t = A_{t-1} y_{t-1} + A_t x_t.$$

Unroll it, we get:

$$A_t y_t - A_{t-1} y_{t-1} = A_t x_t, \ldots, A_2 y_2 - A_1 y_1 = A_2 x_2. \tag{5}$$

To derive an expression for y_t, we sum the recursive equations and obtain:

$$A_t y_t - A_1 y_1 = \sum_{s=2}^{t} A_s c x_s, y_t A_t = \sum_{s=1}^{t} A_s x_s, y_t = \sum_{s=1}^{t} \frac{A_s}{A_t} x_s. \tag{6}$$

By comparing the coefficients, we can obtain $c_{ts} = A_s / A_t$.

$\Leftarrow$:

Given the linear combination $y_t = \sum_{s=1}^{t} c_{ts} x_s$ and $c_{ts} = \frac{g_s}{g_t}$, we define $a_t \triangleq \frac{g_{t-1}}{g_t}$. Then y_t can be expressed as:

$$\begin{aligned} y_t &= \sum_{s=1}^{t} c_{ts} x_s = \sum_{s=1}^{t-1} c_{ts} x_s + c_{tt} x_t = \sum_{s=1}^{t-1} \frac{g_s}{g_t} x_s + \frac{g_t}{g_t} x_t \\ &= \frac{g_{t-1}}{g_t} \sum_{s=1}^{t-1} \frac{g_s}{g_{t-1}} x_s + x_t = a_t \sum_{s=1}^{t-1} c_{t-1,s} x_s + x_t = a_t y_{t-1} + x_t. \quad \square \end{aligned}$$

Based on the Theorem 4.1, for linear recurrence, we can directly discuss g_t, as a_t can be obtained through $\frac{g_{t-1}}{g_t}$. Intuitively, g_t can be interpreted as an importance score up to moment t, $c_{ts} = \frac{g_s}{g_t}$ can be interpreted

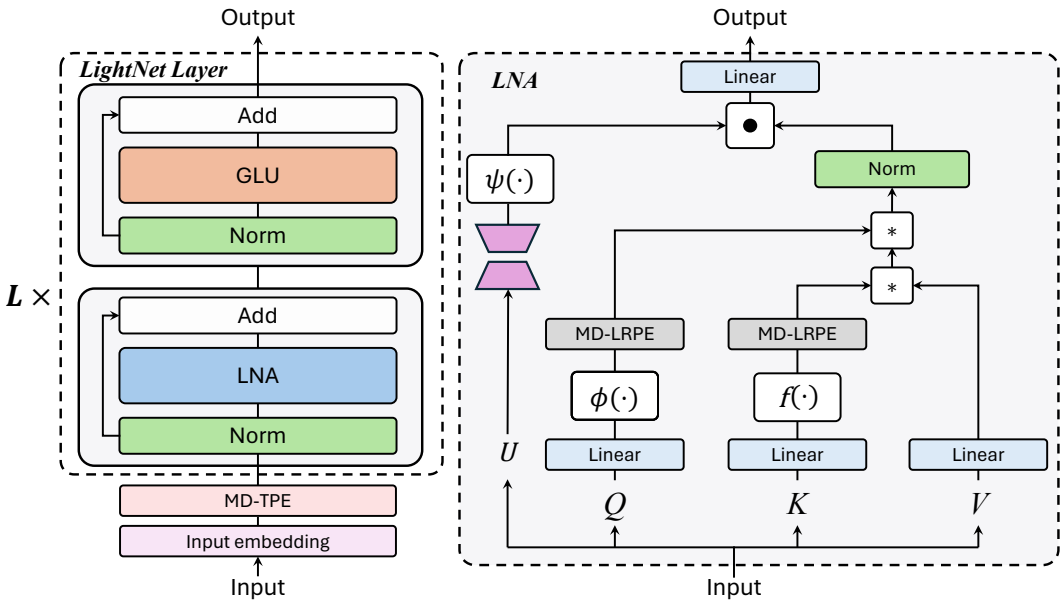

Figure 3: **The network structure of LightNet**: each LightNet model is comprised of an Input Embedding, MD-TPE, and a stack of multiple LightNet Layers. Each LightNet Layer consists of an LNA and a GLU, with the computation of LNA illustrated in the figure on the right.

as the ratio of the score at moment s relative to moment t, and a_t can be interpreted as the ratio of the previous moment's score to moment t's score.

Typically, to prevent numerical overflow, we assume $0 \leq a_t = \frac{g_{t-1}}{g_t} \leq 1$. To meet this condition, we present the following two forms:

Proposition 4.2. *For Linear Recurrence with* $0 \leq a_t \leq 1$*, there exist two forms:*
1. Multiplicative decay: $\log g_t = \log g_{t-1} + \delta_t, a_t = \exp(-\delta_t)$*;*
2. Additive decay: $g_t = g_{t-1} + \delta_t, a_t = \frac{\sum_{s=1}^{t-1} \delta_s}{\sum_{s=1}^{t} \delta_s}$*;*
where $\delta_t \triangleq \delta(x_t) \geq 0$.

Proof of Proposition 4.2. The condition $0 \leq \frac{g_{t-1}}{g_t} \leq 1$, is equivalent to $\delta_t = \log g_t - \log g_{t-1} \geq 0$ or $\delta_t = g_t - g_{t-1} \geq 0$. The former formula brings the multiplicative type, while the latter delivers the additive type. □

It can be observed that the typical linear attention with decay corresponds to the Multiplicative decay, where δ_t is utilized as Softplus(·) (Yang et al., 2023; Gu & Dao, 2023), exp(·)) (Gu & Dao, 2023), or a fixed value (Qin et al., 2023a; Sun et al., 2023c). Since the a_t in Multiplicative decay depends solely on the input x_t at the current timestep, a single scan cannot enable y_t to capture the information from $x_1, \ldots, x_n$ (n is the sequence length), i.e., the global context, when processing high-dimensional data. However, for the Additive decay, since the computation decay is $a_t = \frac{\sum_{s=1}^{t-1} \delta_s}{\sum_{s=1}^{t} \delta_s}$, by modifying the denominator to $\Delta = \sum_{s=1}^{n} \delta_s$, global information can be obtained through $a_t = \frac{\sum_{s=1}^{t-1} \delta_s}{\Delta}$.

5 LightNet

Building upon the preceding analysis, we introduce a novel Linear Transformer architecture termed **LightNet**, designed to handle multi-dimensional data efficiently in 1 scan. An overview of its structure is depicted in Fig. 3. LightNet comprises an Input Embedding, MD-TPE module, and several stacked LightNet Layers.

5.1 LightNet Layer

The LightNet Layer is composed of a LightNet Attention (LNA) and a Gated Linear Unit (GLU) (Shazeer, 2020). Within the LNA, an additive decay is employed, with δ implemented through the exponential function. Additionally, a parameter sharing strategy (Qin et al., 2024b) is utilized for both the key and decay, which has been empirically observed to enhance performance. This empirical evidence is detailed in Table 4. Furthermore, the integration of a low-rank output gate from TNL3 (Qin et al., 2023a) and a normalization after linear attention (Qin et al., 2022) has been incorporated.

In causal settings, the LightNet Layer can be represented as follows:

$$\begin{aligned} \mathbf{s}_t = \mathbf{s}_{t-1} + \exp(\mathbf{k}_t), \bar{\mathbf{k}}_\mathbf{t} = \exp(\mathbf{k}_t)/\mathbf{s}_t, \mathbf{kv}_t = \operatorname{diag}\{1 - \bar{\mathbf{k}}_\mathbf{t}\}\mathbf{kv}_{t-1} + \bar{\mathbf{k}}_\mathbf{t}\mathbf{v}_t^\top, \\ \mathbf{o}_t^\top = \operatorname{Norm}[\mathbf{kv}_t^\top \phi(\mathbf{q}_t)] \odot \psi(u_t). \end{aligned} \tag{7}$$

In non-causal settings, the expression becomes:

$$\begin{aligned} \mathbf{s} = \sum_t \exp(\mathbf{k}_t), \mathbf{o}_t = \operatorname{Norm}\left[\phi(q_t)\sum_t (\exp(k_t)/s)^\top \mathbf{v}_t\right] \odot \psi(u_t), \\ \mathbf{O} = \operatorname{Norm}\left[\phi(\mathbf{Q})(f(\mathbf{K})^\top \mathbf{V})\right] \odot \psi(\mathbf{U}). \end{aligned} \tag{8}$$

where $\mathbf{X}$ is the input of LNA, $\mathbf{W}_q, \mathbf{W}_k, \mathbf{W}_v$ are linear projection matrices and $\mathbf{W}_{u1}, \mathbf{W}_{u2}$ are low rank projection of output gates:

$$\mathbf{Q} = \mathbf{X}\mathbf{W}_q, \mathbf{K} = \mathbf{X}\mathbf{W}_k, \mathbf{V} = \mathbf{X}\mathbf{W}_v, \mathbf{U} = \mathbf{X}\mathbf{W}_{u1}\mathbf{W}_{u2}, \phi = \text{Swish}, \psi = \text{Sigmoid}, f = \text{Softmax}. \tag{9}$$

5.2 Multi Dimension Position Encoding

It is noted that additive decay recurrence does not have a locality prior like multiplicative decay recurrence and is permutation invariant in non-causal scenarios, as shown in E.q 8. Therefore, it is necessary to introduce new positional encoding. We choose to use relative positional encoding due to its superior performance compared to absolute positional encoding (Shaw et al., 2018). However, existing relative positional encoding methods for Transformers are incompatible with LightNet, as they either require direct manipulation of the attention scores (Shaw et al., 2018) or fail to retain the benefits of relative positional information (Su et al., 2021). For detailed discussions, see Appendix A.2. This necessitates designing a positional encoding scheme tailored for LightNet. To tackle this challenge, we introduce two novel relative positional encoding methods, MD-TPE (Multi-Dimensional Toeplitz Positional Encoding) and MD-LRPE (Multi-Dimensional Linearized Relative Positional Encoding), which is the high-dimensional context expanding of the LRPE (Qin et al., 2023b). This expanding of MD-LRPE enables the management of relative positional relationships in any dimension.

MD-TPE. Given multi-dimension input $\mathbf{x}_{n_1,\ldots,n_k}, 1 \le n_s \le N_s, s = 1, \ldots k$, we use the following equation to capture relative positional information:

$$\mathbf{y}_{n_1,\ldots,n_k} = \sum_{m_k \le n_k} \cdots \sum_{m_1 \le n_1} \mathbf{t}_{n_1-m_1,\ldots,n_k-m_k} \mathbf{x}_{m_1,\ldots,m_k}. \tag{10}$$

However, the time complexity of implementing the aforementioned method is $O(N \log N)$, where $N = \prod_{s=1}^{k} n_s$, making it inefficient. To address this, we simplified the above formula by performing toeplitz matrix production for each dimension separately and using SSM for parameterization (Qin & Zhong, 2023; Gu et al., 2021; Ma et al., 2023; 2024), we denote e as the hidden dimension of SSM below:

$$\mathbf{y}_{n_1,\ldots,n_k} = \sum_{s=1}^{k} \sum_{m_s=1}^{n_s} \mathbf{t}_{n_s-m_s} \mathbf{x}_{n_1,\ldots,m_s,\ldots,n_k} = \sum_{s=1}^{k} \sum_{m_s=1}^{n_s} \sum_{r=1}^{e} \lambda_r^{n_s-m_s} \mathbf{x}_{n_1,\ldots,m_s,\ldots,n_k}. \tag{11}$$

Where λ_r is decay factor for t-th feature of SSM. By using a scan approach, the above calculation becomes linear in complexity, $O(Ne)$.

Table 1: **Performance comparison for image classification task on ImageNet1k.** "S.A." represents Softmax Attention, "M.S." denotes multiple scans, and "O.S." signifies one scan. The best result is highlighted with **bold** and the second with underlined.

Model	Category	Tiny		Small		Base	
		Acc (%) ↑	Params (M)	Acc (%) ↑	Params (M)	Acc (%) ↑	Params (M)
DeiT (Touvron et al., 2021)	S.A.	72.20	5.7	79.90	22.00	81.80	86.00
Hgrn (Qin et al., 2024c)	M.S.	74.40	6.1	80.09	23.70	-	-
Vim (Zhu et al., 2024)	M.S.	**76.10**	7.0	**80.50**	26.00	-	-
V-RWKV (Duan et al., 2024)	M.S.	75.10	6.2	80.10	23.80	**82.00**	93.70
Tnl (RetNet) (Qin et al., 2023a)	M.S.	72.89	6.0	78.76	22.56	80.62	87.59
Hgrn2 (Qin et al., 2024b)	M.S.	75.39	6.1	80.12	23.80	-	-
LightNet	O.S.	74.46	6.0	80.12	22.64	81.90	87.74
LightNet w/o TPE	O.S.	73.97	6.0	79.65	22.54	81.45	87.54
LightNet w/o LRPE	O.S.	74.02	6.0	79.54	22.63	81.72	87.69
LightNet w/o Decay	O.S.	71.85	6.0	79.95	22.64	80.71	87.74

Table 2: **Performance Scores on GLUE Benchmark.** We utilize the Cramming-BERT 24-hour training configuration and observe that LightNet outperforms Crammed BERT and achieves comparable results to BERT-Base, which is trained with more GPU hours. The best result is highlighted with **bold** and the second with underlined.

Model	**MNLI**	**SST-2**	**STSB**	**RTE**	**QNLI**	**QQP**	**MRPC**	**CoLA**	**GLUE**
BERT-Base (Fully trained)	83.2 / 83.4	91.9	**86.7**	**59.2**	**90.6**	**87.7**	**89.3**	**56.5**	**80.9**
BERT-Base (No Pretrain)	34.1 / 34.1	79.9	17.8	47.3	50.0	68.6	77.9	-	45.5
Crammed BERT	**83.9** / **84.1**	92.2	84.6	53.8	89.5	87.3	87.5	44.5	78.6
LightNet	83.3 / 83.5	**92.9**	86.3	55.6	89.1	**87.7**	88.5	52.6	79.9
LightNet w/o TPE	82.1 / 82.9	92.4	79.4	57.8	89.2	**87.7**	83.8	44.1	77.7
LightNet w/o LRPE	82.0 / 82.7	92.7	76.3	57.4	88.5	87.5	83.8	38.2	76.6

MD-LRPE. Given $\mathbf{x}_t \in \mathbb{R}^d, \mathbf{x} \in \{\mathbf{q}, \mathbf{k}\}$, LRPE transforms it through the matrix $\mathbf{W}_t$ to $\mathbf{W}_t\mathbf{x}_t, \mathbf{x} \in \{\mathbf{q}, \mathbf{k}\}$, and it holds that:

$$(\mathbf{W}_s\mathbf{q}_s)^{\mathrm{H}}(\mathbf{W}_t\mathbf{k}_t) = \mathbf{q}_s^{\mathrm{H}}\mathbf{W}_s^{\mathrm{H}}\mathbf{W}_t\mathbf{k}_t = \mathbf{q}_s^{\mathrm{H}}\mathbf{W}_{t-s}\mathbf{k}_t. \tag{12}$$

We choose the complex version of LRPE, where:

$$\mathbf{W}_t = \mathrm{diag}\{\exp(it\theta_1), \ldots, \exp(it\theta_d)\}. \tag{13}$$

To generalize to higher dimensions, *i.e.*, given $\mathbf{x}_{n_1,\ldots,n_k} \in \mathbb{R}^d, \mathbf{x} \in \{\mathbf{q}, \mathbf{k}\}$, we divide the d features into k groups, each group has d/k features, with the s-th group's features corresponding to dimension n_s, $s \in [1, k]$. Specifically, we define:

$$\mathbf{W}_{n_1,\ldots,n_k} = \mathrm{diag}\{[\Theta_1, \ldots, \Theta_k]\}, \Theta_s = \exp(in_k\theta_j), sd/k < j \leq (s+1)d/k, \theta_j = 10000^{-2j/d}. \tag{14}$$

Thus:
$$\mathbf{W}^{\mathbf{H}}_{n_1,\ldots,n_k}\mathbf{W}_{m_1,\ldots,m_k} = \mathbf{W}_{m_1-n_1,\ldots,m_k-n_k} \tag{15}$$

Then:
$$\begin{aligned}(\mathbf{W}_{n_1,\ldots,n_k}\mathbf{q}_{n_1,\ldots,n_k})^{\mathrm{H}}(\mathbf{W}_{m_1,\ldots,m_k}\mathbf{k}_{m_1,\ldots,m_k}) &= \mathbf{q}^{\mathrm{H}}_{n_1,\ldots,n_k}\mathbf{W}_s^{\mathrm{H}}\mathbf{W}_t\mathbf{k}_{m_1,\ldots,m_k} \\ &= \mathbf{q}^{\mathrm{H}}_{n_1,\ldots,n_k}\mathbf{W}_{m_1-n_1,\ldots,m_k-n_k}\mathbf{k}_{m_1,\ldots,m_k}.\end{aligned} \tag{16}$$

6 Experiments

We comprehensively evaluate the substitutability of our LightNet in performance, scalability, flexibility, and efficiency. We validate the effectiveness of our model on various multi-dimensional sequential modeling tasks. We also test the proposed ability of LightNet to serve as a language model.

6.1 Setting

Image Classification. We trained our LightNet model for image classification on the ImageNet-1K dataset (Deng et al., 2009). Our approach modifies the network architecture and training protocols of DeiT (Touvron et al., 2021), substituting its Transformer Layers with our proprietary LightNet Layers.

Image Generation. We build our model upon the latent diffusion model (Rombach et al., 2022; Peebles & Xie, 2023) and use our proposed LightNet as the denoising network. We adjust the model size across various configurations (S, B, L, XL) and patch sizes (8, 4, 2), consistent with DiT (Peebles & Xie, 2023). Experiments are conducted on the ImageNet dataset (Deng et al., 2009) at a resolution of 256 × 256. We compare the performance with typical methods for image generation, CDM (Ho et al., 2022), LDM (Rombach et al., 2022), and DiT (Peebles & Xie, 2023). Each model is trained over 0.4M steps with a batch size of 256 to assess scaling capabilities. For the largest model variant, training is extended to 0.8M steps with a batch size of 1024, as opposed to the 7M steps in DiT, to enhance generative performance.

Table 3: **Performance comparison for image generation task on ImageNet-1k.** LightNet-XL/2 achieves state-of-the-art FID with or without classifier-free guidance (-G).The best result is highlighted with **bold** and the second with underlined.

Model	FID↓	sFID↓	IS↑	Precision↑	Recall↑	Params
CDM	4.88	-	158.71	-	-	-
LDM-8	15.51	-	79.03	0.65	0.63	395M
LDM-8-G	7.76	-	209.52	<u>0.84</u>	0.35	506M
LDM-4	10.56	-	103.49	0.71	0.62	400M
LDM-4-G	3.60	-	247.67	**0.87**	0.48	400M
DiT-XL/2	9.62	6.85	121.50	0.67	**0.67**	675M
DiT-XL/2-G	<u>2.27</u>	<u>4.60</u>	<u>278.24</u>	0.83	0.57	675M
LightNet-XL/2	5.35	5.93	171.18	0.73	<u>0.65</u>	672M
LightNet-XL/2-G	**2.18**	**4.58**	**281.85**	0.83	0.58	672M

Bidirectional Language Modeling. We utilize Cramming-BERT (Geiping & Goldstein, 2022) as our pipeline, employing a 24-hour training regime to pretrain on the Pile dataset, subsequently finetuning on the GLUE benchmark (Wang et al., 2018). During pretraining, we follow established guidelines by setting a learning rate of 1e-3, a sequence length of 128, and a batch size of 8192. In the finetuning phase, we experiment with learning rates from the set {5e-5, 4e-5, 3e-5, 2e-5} and determine the optimal outcome by finetuning over 5 epochs.

Autoregressive Language Modeling. We evaluate two capabilities: perplexity (PPL) and zero-shot reasoning ability. The perplexity of the 44M model is assessed on the Wikitext-103 dataset (Merity et al., 2016), and the 380M model's perplexity is tested on the Pile dataset, consuming 10 billion tokens . For large language model experiments, we train LightNet models at scales of 1B, and 3B using 300 billion tokens sampled from subsets of the Pile (Gao et al., 2020). These models are then evaluated on commonsense reasoning tasks using the lm-eval-harness (Gao et al., 2021). Detailed training hyperparameters are listed in Table 11.

Table 4: **Performance comparison on Wikitext-103**. ↓ means *lower is better*. We adopted the configuration of HGRN for Wikitext-103, and we can observe that LightNet significantly outperforms all other methods. The best result is highlighted with **bold** and the second with underlined.

Model	PPL (val) ↓	PPL (test) ↓	Params (M)
Attn-based			
Transformer	24.40	24.78	44.65
FLASH	25.92	26.70	42.17
1+elu	27.44	28.05	44.65
Performer	62.50	63.16	44.65
cosFormer	26.53	27.06	44.65
RNN-based			
S4	38.34	39.66	45.69
DSS	39.39	41.07	45.73
GSS	29.61	30.74	43.84
RWKV-4	24.31	25.07	46.23
LRU	29.86	31.12	46.24
HGRN	24.14	24.82	46.25
FFT-based			
TNN	<u>23.98</u>	<u>24.67</u>	48.68
LightNet	**23.09**	**23.75**	45.07

6.2 Results

Image Classification. As shown in Table 1, the proposed LightNet shows competitive performance on the ImageNet-1k dataset. It can be observed that using only a single sequential scan, LightNet can achieve comparable performance to models with naive attention and multiple sequential scans.

Image Generation. The image generation results are presented in Table 3. Our proposed LightNet demonstrates superior performance, achieving a lower Fréchet Inception Distance (FID) and a higher Inception Score (IS) than DiT (Peebles & Xie, 2023) with fewer training steps (0.8M steps vs 7M steps). Additionally, LightNet exhibits commendable scaling capabilities, as illustrated in Fig. 4.

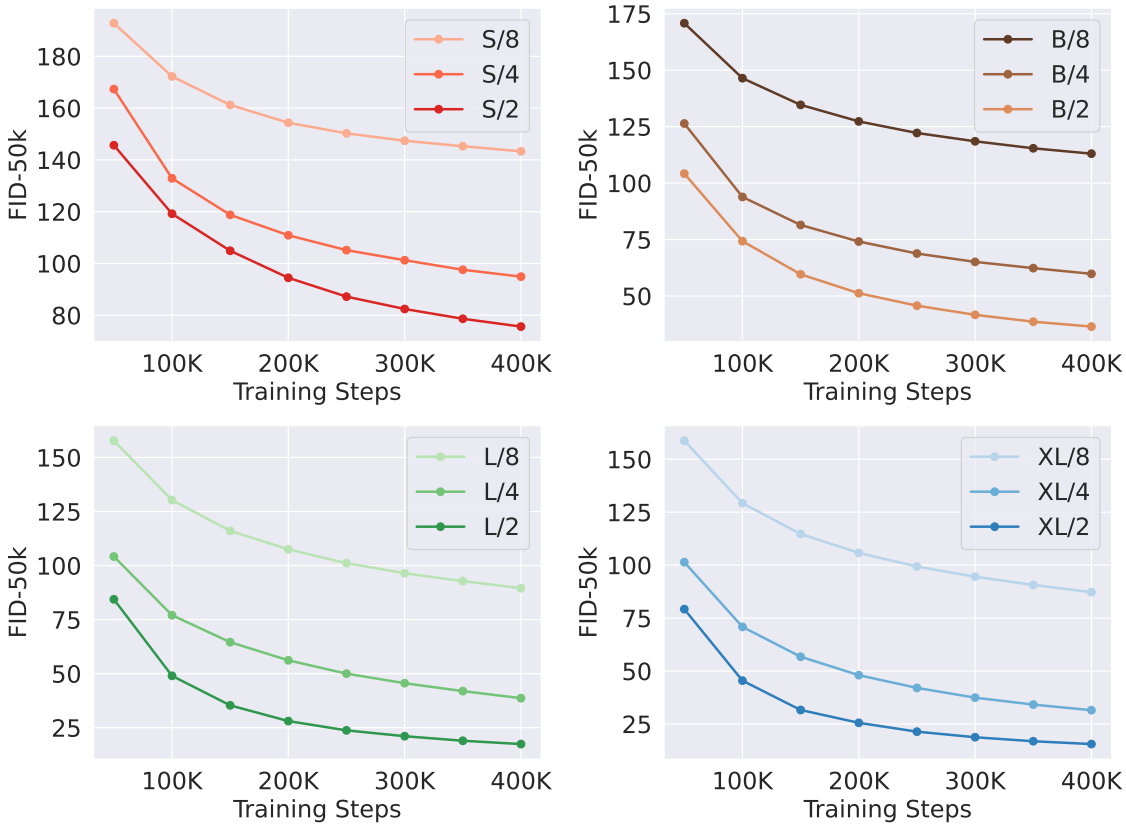

Figure 4: **Scaling up the LightNet enhances the FID during every stages of training.** We present the FID-50K across training iterations for twelve LightNet models. Enhancing the LightNet backbone results in improved generative models for all sizes of models and patches.

Bidirectional Language Modeling. As shown in Table 2, LightNet outperforms Crammed Bert (Geiping & Goldstein, 2022) on the GLUE dataset, demonstrating its superior capability in handling natural language understanding tasks. Despite BERT-Base (Devlin et al., 2019) achieving comparable performance, it is noteworthy that LightNet does so with a significantly lower computational cost, having been trained on a single A100 for 24 hours.

Autoregressive Language Modeling. In the Wikitext-103 dataset, as depicted in Table 4, LightNet surpasses all competitors on both the validation and test datasets. Regarding large-scale datasets, as illustrated in Table 5, LightNet exhibits superior perplexity (PPL) compared to LLaMA (Touvron et al., 2023) and TNL (Qin et al., 2023a), and matches the performance of Mamba (Gu & Dao, 2023). The ability of LightNet to achieve high performance with reduced parameter complexity underscores its potential for scalability and broader application across various large-scale data scenarios. For the results of the 1B and 3B models, please refer to Table 8. For the retrieval results, please refer to Figure 5.

Table 5: **Performance comparison Pile for large-scale language modeling**. We trained under the 10 billion token subset of Pile, and it can be seen that LightNet's PPL is better than LLaMA's. The best result is highlighted with **bold** and the second with underlined.

Model	PPL ↓	Params
LLaMA	<u>4.62</u>	385M
TNL	<u>4.62</u>	379M
Mamba	**4.59**	385M
LightNet	**4.59**	379M
LightNet w/o TPE	4.69	379M
LightNet w/o LRPE	4.69	379M
LightNet no share	4.76	385M
LightNet w/o Decay	4.62	379M

6.3 Ablation Studies

Effectiveness of Parameters Sharing. As discussed in Sec. 5.2, we employ a parameter sharing strategy between decay and key, and the performance comparison is presented in Table 5. The results demonstrate that employing in-

Table 6: **Ablation studies on image classification task** on normalization and low-rank output gate.

Model	Tiny		Small		Base	
	Acc (%) ↑	Params (M)	Acc (%) ↑	Params (M)	Acc (%) ↑	Params (M)
LightNet	74.46	6.00	80.12	22.64	81.90	87.74
LightNet w/o Norm	73.46	6.00	79.65	22.63	81.49	87.72
LightNet w full rank output gate	73.92	6.16	80.04	23.82	81.95	93.64

Table 7: **Ablation studies on image generation** for LightNet-B/2 Configurations. We compare the performance of FID under different training steps.

Model	50K	100K	150K	200K	250K	300K	350K	400K
LightNet-B/2	104.19	74.27	59.60	51.22	45.70	41.65	38.60	36.45
LightNet-B/2 w/o TPE	105.86	77.64	64.81	57.24	51.98	48.12	44.90	42.74
LightNet-B/2 w/o LRPE	132.17	82.99	67.79	59.02	52.88	48.41	44.94	42.37

dependent parameters for decay and key leads to performance deterioration, highlighting the significance of parameter sharing.

Effectiveness of MD-TPE. The proposed MD-TPE provides relative positional information under linear complexity. We thus explore the effectiveness of the MD-TPE across all tasks, shown in Table 1,2,5,7. We can observe that removing MD-TPE results in significant performance degradation, particularly for image generation, which highly depends on the relative position of the image content. Similarly, performance comparison in language modeling tasks also confirms the effectiveness of MD-TPE when reduced to a single dimension.

Effectiveness of MD-LRPE. LRPE has already proven its effectiveness in the field of language modeling. Therefore, when faced with higher-dimensional inputs, the contributions of its extension, MD-LRPE should be systematically validated. To this end, we conduct numerous ablation experiments, and the results, as shown in Table 1,2,5,7, demonstrate the effectiveness of extending LRPE into a multi-dimensional space through MD-LRPE operation.

Normalization and Low Rank output gate. As shown in Table 6, the performance of the low-rank output gate we used in LightNet is comparable to that of the full-rank output gate, with approximately 5% fewer parameters. Moreover, removing the extra-normalization in LightNet significantly decreases the model's effectiveness.

Effectiveness of Additive Decay. We discuss the roles of Additive Decay in the causal setting and the non-causal setting. In Table 1, 5, 8, "LightNet w/o Decay" refers to removing Additive Decay and using the "SiLU" activation function. For the causal setting, we evaluate the impact of removing Additive Decay in language models. The results, as shown in Table 5, 8, reveal that removing Additive Decay decreases the perplexity (PPL) by 0.03. For 1B and 3B parameter language models, removing Additive Decay reduces accuracy on Commonsense Reasoning Tasks by approximately 2%. In the non-causal setting, we test classification performance on ImageNet. As shown in Table 1, removing the Additive Decay (i.e., "Softmax" activation function is this scenery) leads to significant performance degradation across all models. This demonstrates the critical role of the Softmax activation function in non-causal tasks. **Speed Test.** The current linear complexity models employ multiplicative linear recurrence in sequence modeling and necessitate at least two scans for multi-dimensional data, resulting in processing time denoted by the "2 Scan" in Fig. 2. In contrast, our LightNet requires only a single scan, leading to a processing time denoted by the "1 Scan". As evident from the figure, the advantage of the "1 Scan" becomes increasingly pronounced with the growth of sequence length.

7 Conclusion

In this paper, we have addressed the inefficiency of "multiplicative decay" linear recurrence in multi-dimensional sequence modeling by introducing a novel "additive decay" linear recurrence that handles multi-dimensional data within a single scan. We developed LightNet, a new multi-dimensional linear attention model enhanced by two new multi-dimensional linear relative positional encoding methods, MD-TPE and MD-LRPE. Empirical evaluations across tasks like image classification, image generation, bidirectional language modeling, and autoregressive language modeling demonstrate LightNet's superior performance and versatility. LightNet offers a significant advancement in efficiency and scalability, providing a promising pathway for future research and applications in multi-dimensional sequence modeling.

References

Jimmy Lei Ba, Jamie Ryan Kiros, and Geoffrey E. Hinton. Layer normalization, 2016.

Krzysztof Marcin Choromanski, Valerii Likhosherstov, David Dohan, Xingyou Song, Andreea Gane, Tamas Sarlos, Peter Hawkins, Jared Quincy Davis, Afroz Mohiuddin, Lukasz Kaiser, et al. Rethinking attention with performers. In *Proceedings of the International Conference on Learning Representations (ICLR)*, 2020.

Jia Deng, Wei Dong, Richard Socher, Li-Jia Li, Kai Li, and Li Fei-Fei. Imagenet: A large-scale hierarchical image database. In *Proceedings of the IEEE Conference on Computer Vision and Pattern Recognition (CVPR)*, pp. 248–255. Ieee, 2009.

Jacob Devlin, Ming-Wei Chang, Kenton Lee, and Kristina Toutanova. BERT: Pre-training of deep bidirectional transformers for language understanding. In Jill Burstein, Christy Doran, and Thamar Solorio (eds.), *Proceedings of the 2019 Conference of the North American Chapter of the Association for Computational Linguistics: Human Language Technologies, Volume 1 (Long and Short Papers)*, pp. 4171–4186, Minneapolis, Minnesota, June 2019. Association for Computational Linguistics. doi: 10.18653/v1/N19-1423. URL https://aclanthology.org/N19-1423.

Yuchen Duan, Weiyun Wang, Zhe Chen, Xizhou Zhu, Lewei Lu, Tong Lu, Yu Qiao, Hongsheng Li, Jifeng Dai, and Wenhai Wang. Vision-rwkv: Efficient and scalable visual perception with rwkv-like architectures. *arXiv preprint arXiv:2403.02308*, 2024.

Zhengcong Fei, Mingyuan Fan, Changqian Yu, and Junshi Huang. Scalable diffusion models with state space backbone. *arXiv preprint arXiv:2402.05608*, 2024a.

Zhengcong Fei, Mingyuan Fan, Changqian Yu, Debang Li, and Junshi Huang. Diffusion-rwkv: Scaling rwkv-like architectures for diffusion models. *arXiv preprint arXiv:2404.04478*, 2024b.

Leo Gao, Stella Biderman, Sid Black, Laurence Golding, Travis Hoppe, Charles Foster, Jason Phang, Horace He, Anish Thite, Noa Nabeshima, Shawn Presser, and Connor Leahy. The Pile: An 800gb dataset of diverse text for language modeling. *arXiv preprint arXiv:2101.00027*, 2020.

Leo Gao, Jonathan Tow, Stella Biderman, Sid Black, Anthony DiPofi, Charles Foster, Laurence Golding, Jeffrey Hsu, Kyle McDonell, Niklas Muennighoff, Jason Phang, Laria Reynolds, Eric Tang, Anish Thite, Ben Wang, Kevin Wang, and Andy Zou. A framework for few-shot language model evaluation. Zenodo, September 2021. doi: 10.5281/zenodo.5371628. URL https://doi.org/10.5281/zenodo.5371628.

Jonas Geiping and Tom Goldstein. Cramming: Training a language model on a single gpu in one day. *arXiv preprint arXiv:2212.14034*, 2022.

Albert Gu and Tri Dao. Mamba: Linear-time sequence modeling with selective state spaces. *arXiv preprint arXiv:2312.00752*, 2023.

Albert Gu, Karan Goel, and Christopher Re. Efficiently modeling long sequences with structured state spaces. In *Proceedings of the International Conference on Learning Representations (ICLR)*, 2021.

Albert Gu, Karan Goel, Ankit Gupta, and Christopher Ré. On the parameterization and initialization of diagonal state space models. *Proceedings of the Advances in Neural Information Processing Systems (NeurIPS)*, 35:35971–35983, 2022.

Jonathan Ho, Chitwan Saharia, William Chan, David J Fleet, Mohammad Norouzi, and Tim Salimans. Cascaded diffusion models for high fidelity image generation. *Journal of Machine Learning Research (JMLR)*, 23(47):1–33, 2022.

Vincent Tao Hu, Stefan Andreas Baumann, Ming Gui, Olga Grebenkova, Pingchuan Ma, Johannes Fischer, and Bjorn Ommer. Zigma: Zigzag mamba diffusion model. *arXiv preprint arXiv:2403.13802*, 2024.

Angelos Katharopoulos, Apoorv Vyas, Nikolaos Pappas, and François Fleuret. Transformers are rnns: Fast autoregressive transformers with linear attention. In *International Conference on Machine Learning (ICML)*, pp. 5156–5165. PMLR, 2020.

Xuezhe Ma, Chunting Zhou, Xiang Kong, Junxian He, Liangke Gui, Graham Neubig, Jonathan May, and Luke Zettlemoyer. Mega: Moving average equipped gated attention. In *The Eleventh International Conference on Learning Representations*, 2023. URL https://openreview.net/forum?id=qNLe3iq2El.

Xuezhe Ma, Xiaomeng Yang, Wenhan Xiong, Beidi Chen, LILI YU, Hao Zhang, Jonathan May, Luke Zettlemoyer, Omer Levy, and Chunting Zhou. Megalodon: Efficient LLM pretraining and inference with unlimited context length. In *The Thirty-eighth Annual Conference on Neural Information Processing Systems*, 2024. URL https://openreview.net/forum?id=XlAbMZu4Bo.

Eric Martin and Chris Cundy. Parallelizing linear recurrent neural nets over sequence length. In *Proceedings of the International Conference on Learning Representations (ICLR)*. OpenReview.net, 2018. URL https://openreview.net/forum?id=HyUNwulC-.

Harsh Mehta, Ankit Gupta, Ashok Cutkosky, and Behnam Neyshabur. Long range language modeling via gated state spaces. In *Proceedings of the International Conference on Learning Representations (ICLR)*, 2023.

Stephen Merity, Caiming Xiong, James Bradbury, and Richard Socher. Pointer sentinel mixture models. In *Proceedings of the International Conference on Learning Representations (ICLR)*, 2016.

Antonio Orvieto, Samuel L. Smith, Albert Gu, Anushan Fernando, Çaglar Gülçehre, Razvan Pascanu, and Soham De. Resurrecting recurrent neural networks for long sequences. *CoRR*, abs/2303.06349, 2023. doi: 10.48550/arXiv.2303.06349. URL https://doi.org/10.48550/arXiv.2303.06349.

Adam Paszke, Sam Gross, Francisco Massa, Adam Lerer, James Bradbury, Gregory Chanan, Trevor Killeen, Zeming Lin, Natalia Gimelshein, Luca Antiga, Alban Desmaison, Andreas Köpf, Edward Yang, Zach DeVito, Martin Raison, Alykhan Tejani, Sasank Chilamkurthy, Benoit Steiner, Lu Fang, Junjie Bai, and Soumith Chintala. Pytorch: An imperative style, high-performance deep learning library. *arXiv preprint arXiv:1912.01703*, 2019.

William Peebles and Saining Xie. Scalable diffusion models with transformers. In *Proceedings of the IEEE International Conference on Computer Vision (ICCV)*, pp. 4195–4205, 2023.

Bo Peng, Eric Alcaide, Quentin Gregory Anthony, Alon Albalak, Samuel Arcadinho, Stella Biderman, Huanqi Cao, Xin Cheng, Michael Nguyen Chung, Leon Derczynski, et al. Rwkv: Reinventing rnns for the transformer era. In *Proceedings of the Conference on Empirical Methods in Natural Language Processing (EMNLP)*, 2023.

Bo Peng, Daniel Goldstein, Quentin Anthony, Alon Albalak, Eric Alcaide, Stella Biderman, Eugene Cheah, Teddy Ferdinan, Haowen Hou, Przemysław Kazienko, et al. Eagle and finch: Rwkv with matrix-valued states and dynamic recurrence. *arXiv preprint arXiv:2404.05892*, 2024.

Zhen Qin and Yiran Zhong. Accelerating toeplitz neural network with constant-time inference complexity. In *Proceedings of the Conference on Empirical Methods in Natural Language Processing (EMNLP)*, 2023. URL https://openreview.net/forum?id=FAiFBfFTGZ.

Zhen Qin, Weixuan Sun, Hui Deng, Dongxu Li, Yunshen Wei, Baohong Lv, Junjie Yan, Lingpeng Kong, and Yiran Zhong. cosformer: Rethinking softmax in attention. In *Proceedings of the International Conference on Learning Representations (ICLR)*, 2021.

Zhen Qin, Xiaodong Han, Weixuan Sun, Dongxu Li, Lingpeng Kong, Nick Barnes, and Yiran Zhong. The devil in linear transformer. In *Proceedings of the Conference on Empirical Methods in Natural Language Processing (EMNLP)*, pp. 7025–7041, 2022.

Zhen Qin, Dong Li, Weigao Sun, Weixuan Sun, Xuyang Shen, Xiaodong Han, Yunshen Wei, Baohong Lv, Xiao Luo, Yu Qiao, and Yiran Zhong. Transnormerllm: A faster and better large language model with improved transnormer. *arXiv preprint arXiv:2307.14995*, 2023a.

Zhen Qin, Weixuan Sun, Kaiyue Lu, Hui Deng, Dongxu Li, Xiaodong Han, Yuchao Dai, Lingpeng Kong, and Yiran Zhong. Linearized relative positional encoding. *Transactions on Machine Learning Research (TMLR)*, 2023b. ISSN 2835-8856. URL https://openreview.net/forum?id=xoLyps2qWc.

Zhen Qin, Weigao Sun, Dong Li, Xuyang Shen, Weixuan Sun, and Yiran Zhong. Lightning attention-2: A free lunch for handling unlimited sequence lengths in large language models. *arXiv preprint arXiv:2401.04658*, 2024a.

Zhen Qin, Songlin Yang, Weixuan Sun, Xuyang Shen, Dong Li, Weigao Sun, and Yiran Zhong. Hgrn2: Gated linear rnns with state expansion. *arXiv preprint arXiv:2404.07904*, 2024b.

Zhen Qin, Songlin Yang, and Yiran Zhong. Hierarchically gated recurrent neural network for sequence modeling. *Proceedings of the Advances in Neural Information Processing Systems (NeurIPS)*, 36, 2024c.

Robin Rombach, Andreas Blattmann, Dominik Lorenz, Patrick Esser, and Björn Ommer. High-resolution image synthesis with latent diffusion models. In *Proceedings of the IEEE Conference on Computer Vision and Pattern Recognition (CVPR)*, pp. 10684–10695, 2022.

Peter Shaw, Jakob Uszkoreit, and Ashish Vaswani. Self-attention with relative position representations. In *Proceedings of the 2018 Conference of the North American Chapter of the Association for Computational Linguistics: Human Language Technologies, Volume 2 (Short Papers)*, pp. 464–468, New Orleans, Louisiana, June 2018. Association for Computational Linguistics. doi: 10.18653/v1/N18-2074. URL https://aclanthology.org/N18-2074.

Noam Shazeer. Glu variants improve transformer. *arXiv preprint arXiv:2002.05202*, 2020.

Jimmy TH Smith, Andrew Warrington, and Scott Linderman. Simplified state space layers for sequence modeling. In *Proceedings of the International Conference on Learning Representations (ICLR)*, 2022.

Jianlin Su, Yu Lu, Shengfeng Pan, Bo Wen, and Yunfeng Liu. Roformer: Enhanced transformer with rotary position embedding. *arXiv preprint arXiv:2104.09864*, 2021.

Weixuan Sun, Zhen Qin, Hui Deng, Jianyuan Wang, Yi Zhang, Kaihao Zhang, Nick Barnes, Stan Birchfield, Lingpeng Kong, and Yiran Zhong. Vicinity vision transformer. *IEEE Transactions on Pattern Analysis and Machine Intelligence (T-PAMI)*, 2023a.

Yutao Sun, Li Dong, Shaohan Huang, Shuming Ma, Yuqing Xia, Jilong Xue, Jianyong Wang, and Furu Wei. Retentive network: A successor to transformer for large language models. *arXiv preprint arXiv:2307.08621*, 2023b.

Yutao Sun, Li Dong, Shaohan Huang, Shuming Ma, Yutopeg Xia, Jilong Xue, Jianyong Wang, and Furu Wei. Retentive network: A successor to transformer for large language models. *arXiv preprint arXiv:2307.08621*, 2023c.

Hugo Touvron, Matthieu Cord, Matthijs Douze, Francisco Massa, Alexandre Sablayrolles, and Hervé Jégou. Training data-efficient image transformers & distillation through attention. In *International Conference on Machine Learning (ICML)*, pp. 10347–10357. PMLR, 2021.

Hugo Touvron, Thibaut Lavril, Gautier Izacard, Xavier Martinet, Marie-Anne Lachaux, Timothée Lacroix, Baptiste Rozière, Naman Goyal, Eric Hambro, Faisal Azhar, Aurélien Rodriguez, Armand Joulin, Edouard Grave, and Guillaume Lample. Llama: Open and efficient foundation language models. *CoRR*, abs/2302.13971, 2023. doi: 10.48550/ARXIV.2302.13971. URL https://doi.org/10.48550/arXiv.2302.13971.

Ashish Vaswani, Noam Shazeer, Niki Parmar, Jakob Uszkoreit, Llion Jones, Aidan N Gomez, Łukasz Kaiser, and Illia Polosukhin. Attention is all you need. In *Advances in neural information processing systems*, pp. 5998–6008, 2017.

Alex Wang, Amanpreet Singh, Julian Michael, Felix Hill, Omer Levy, and Samuel R. Bowman. Glue: A multi-task benchmark and analysis platform for natural language understanding. *arXiv preprint arXiv:1804.07461*, 2018.

Jing Nathan Yan, Jiatao Gu, and Alexander M. Rush. Diffusion models without attention. *arXiv preprint arXiv:2311.18257*, 2023.

Songlin Yang, Bailin Wang, Yikang Shen, Rameswar Panda, and Yoon Kim. Gated linear attention transformers with hardware-efficient training. *arXiv preprint arXiv:2312.06635*, 2023.

Biao Zhang and Rico Sennrich. Root mean square layer normalization, 2019.

Lianghui Zhu, Bencheng Liao, Qian Zhang, Xinlong Wang, Wenyu Liu, and Xinggang Wang. Vision mamba: Efficient visual representation learning with bidirectional state space model. *arXiv preprint arXiv:2401.09417*, 2024.

A Appendix

A.1 Proof of Eq 4

Note that

$$\begin{gathered} A_t y_t = A_t a_t y_{t-1} + A_t x_t = A_{t-1} y_{t-1} + A_t x_t, \\ A_t y_t - A_{t-1} y_{t-1} = A_t x_t, \\ \dots, \\ A_2 y_2 - A_1 y_1 = A_2 x_2. \end{gathered}$$

By summing up, we can obtain:

$$A_t y_t - A_1 y_1 = \sum_{s=2}^{t} A_s c x_s, y_t A_t = \sum_{s=1}^{t} A_s x_s, y_t = \sum_{s=1}^{t} \frac{A_s}{A_t} x_s.$$

A.2 Further Discussions on Relative Positional Encoding

In this section, we discuss why mainstream relative positional encodings (RPEs) are unsuitable for LightNet. We categorize the main types of RPEs into **Additive RPE** and **Multiplicative RPE** (Qin et al., 2023b) (note that these should not be confused with the "Additive decay" and "Multiplicative decay" linear recurrence discussed in this paper).

Additive RPE Additive RPE (Shaw et al., 2018) is typically expressed in the following form. To simplify the discussion, we omit the scaling factors. Here, $w_{t-s} \in \mathbb{R}$ represents the relative positional encoding:

$$a_{ts} = \mathbf{q}_t^\top \mathbf{k}_s + w_{t-s}, \mathbf{o}_t = \sum_s \frac{\exp(a_{ts})}{\sum_s \exp(a_{ts})} \mathbf{v}_s.$$

As shown, Additive RPE requires computation of the attention scores, which is not allowed in LightNet due to compute $\mathbf{K}^\top \mathbf{V}$ first, (Katharopoulos et al., 2020).

Multiplicative RPE The representative work of Multiplicative RPE is RoPE (Su et al., 2021). Although RoPE does not require direct computation of attention scores, it fails to preserve relative positional information when applied to LightNet. Specifically:

$$\begin{aligned} \mathbf{o}_t^\top &= \sum_{s \le t} \mathbf{q}_t^\top \mathbf{W}_t^\top \left(\frac{\mathbf{W}_s \exp(\mathbf{k}_s)}{\sum_{j=1}^{t} \exp(\mathbf{k}_j)} \right) \mathbf{v}_s^\top \\ &= \sum_{s \le t} \mathbf{q}_t^\top \mathbf{W}_t^\top \operatorname{diag} \left(\sum_{j=1}^{t} \exp(\mathbf{k}_j) \right)^{-1} (\mathbf{W}_s \exp(\mathbf{k}_s)) \, \mathbf{v}_s^\top \\ &\neq \sum_{s \le t} \mathbf{q}_t^\top \mathbf{W}_t^\top \mathbf{W}_s \operatorname{diag} \left(\sum_{j=1}^{t} \exp(\mathbf{k}_j) \right)^{-1} \exp(\mathbf{k}_s) \mathbf{v}_s^\top \\ &= \sum_{s \le t} \mathbf{q}_t^\top \mathbf{W}_{t-s}^\top \operatorname{diag} \left(\sum_{j=1}^{t} \exp(\mathbf{k}_j) \right)^{-1} \exp(\mathbf{k}_s) \mathbf{v}_s^\top. \end{aligned}$$

Here, $\mathbf{W}_t$ represents the rotation matrix in RoPE. The inequality in the second-to-last step arises because **block-diagonal matrices (RoPE matrices) and diagonal matrices are non-commutative**.

Why LRPE is Chosen The above issue does not arise in LRPE (Qin et al., 2023b), which is implemented as:

$$f_{\text{lrpe}}(\mathbf{x}_t, \Theta) = \operatorname{concat}([\mathbf{x} \odot \cos(t\Theta), \mathbf{x} \odot \sin(t\Theta)], \dim = -1).$$

Thus, the computation becomes:

$$\begin{aligned}\mathbf{o}_t^\top &= \sum_{s\le t}[\mathbf{q}_t \odot \cos(t\Theta), \mathbf{q}_t \odot \sin(t\Theta)]^\top \left[\frac{\exp(\mathbf{k}_s)\odot\cos(s\Theta)}{\sum_{j=1}^t \exp(\mathbf{k}_j)}, \frac{\exp(\mathbf{k}_s)\odot\sin(s\Theta)}{\sum_{j=1}^t \exp(\mathbf{k}_j)}\right]\mathbf{v}_s^\top \\ &= \sum_{s\le t}\mathbf{q}_t^\top \operatorname{diag}\{\cos((t-s)\Theta)\}\frac{\exp(\mathbf{k}_s)}{\sum_{j=1}^t \exp(\mathbf{k}_j)}\mathbf{v}_s^\top.\end{aligned}$$

This demonstrates that LRPE effectively captures relative positional information, making it suitable for LightNet. Hence, we adopt LRPE in our design.

A.3 More experiments

In this section, we provide additional experimental results. In Table 8, we show the performance of LightNet under the Commonsense Reasoning Tasks. In Table 9, we present the advantages of LightNet (1 scan) compared to the 2-scan method. In Table 10, we present the effects of LightNet on image generation tasks across various sizes. In Figure 5, we illustrate the retrieval advantages of LightNet compared to Mamba2.

Table 8: **Performance Comparison on Commonsense Reasoning Tasks.** PS, T, HS, WG stand for parameter size (billion), tokens (billion), HellaSwag, and WinoGrande, respectively.

Model	P	T	PIQA	HS	WG	ARC-e	ARC-c	OBQA	AVG
OPT	2.7	300	73.83	60.60	61.01	60.77	31.31	35.2.0	53.79
Pythia	2.8	300	74.10	59.31	59.91	64.14	33.02	35.60	54.35
BLOOM	3.0	350	70.57	54.53	58.48	59.43	30.38	32.20	50.93
RWKV-4	3.0	-	72.42	58.75	57.30	62.92	35.15	36.20	53.79
LightNet	3.0	300	75.14	60.00	59.75	65.99	33.87	35.80	55.09
LightNet w/o Decay	3.0	300	74.27	57.38	57.30	63.22	31.40	35.20	53.13
LightNet	1.0	300	71.06	47.27	51.30	56.31	27.56	33.00	47.75
LightNet w/o Decay	1.0	300	70.73	45.55	50.51	55.22	27.30	31.00	46.72

Table 9: Performance comparison for image generation task on ImageNet1k, where LightNet use 1 scan, Tnl/RetNet and Hgrn2 use 2 scan.

Model	50K	100K	150K	200K	250K	300K	350K	400K
LightNet-B/8	170.79	146.43	134.63	127.31	122.18	118.50	115.40	113.02
Tnl/RetNet-S/8	178.96	150.09	136.36	127.92	122.77	118.92	115.64	113.36
Hgrn2-S/8	182.75	152.13	140.94	133.95	129.14	125.78	123.27	121.08

A.4 Configurations

In this section, we provide training configurations for all experiments. The configuration for Bidirectional Language Modeling is the same as (Geiping & Goldstein, 2022), while the configurations for the other experiments are as shown in Table 11, 12, 13, 14. We use Pytorch (Paszke et al., 2019) and A100 for training.

Table 10: Performance Metrics Across Different LightNet Configurations

Model	50K	100K	150K	200K	250K	300K	350K	400K
LightNet-S/8	192.79	172.23	161.23	154.34	150.25	147.40	145.27	143.31
LightNet-S/4	167.33	132.89	118.77	110.88	105.15	101.25	97.56	94.90
LightNet-S/2	145.66	119.20	104.90	94.45	87.18	82.41	78.63	75.61
DiT-S/2	-	-	-	-	-	-	-	67.16
LightNet-B/8	170.79	146.43	134.63	127.31	122.18	118.50	115.40	113.02
LightNet-B/4	126.37	93.86	81.44	74.11	68.80	65.09	62.34	59.81
LightNet-B/2	104.19	74.27	59.60	51.22	45.70	41.65	38.60	36.45
DiT-B/2	-	-	-	-	-	-	-	42.76
LightNet-L/8	157.76	130.29	116.06	107.50	101.10	96.47	92.79	89.51
LightNet-L/4	104.18	77.02	64.55	56.16	49.99	45.58	41.91	37.54
LightNet-L/2	84.38	48.98	35.32	28.05	23.75	21.06	18.94	17.42
DiT-L/2	-	-	-	-	-	-	-	24.37
LightNet-XL/8	158.75	129.23	114.72	105.75	99.35	94.53	90.66	87.22
LightNet-XL/4	101.39	70.84	56.75	48.04	42.04	37.43	34.16	31.51
LightNet-XL/2	79.22	45.46	31.61	25.55	21.37	18.74	16.84	15.52
DiT-XL/2	-	-	-	-	-	-	-	19.20

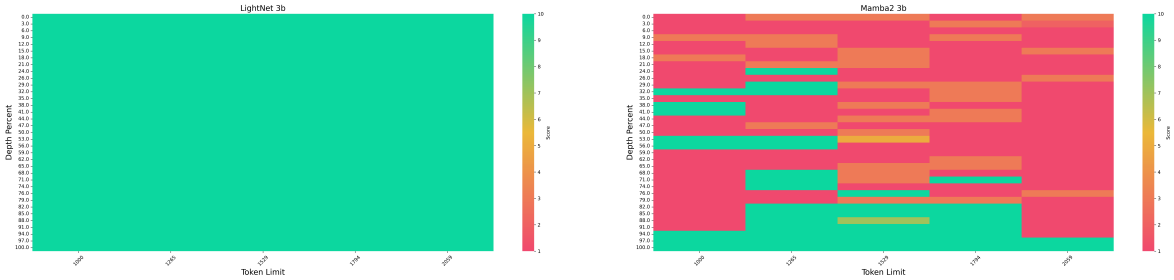

Figure 5: *The Needle-in-the-Haystack results of LightNet and Mamba2, all outcomes were evaluated using GPT, where higher scores indicate better performance. Following (Qin et al., 2024b), we used the easy model, as it is more compatible with the base model. The results demonstrate that LightNet outperforms Mamba2.*

Table 11: **Comprehensive Configurations of the Model and Training Procedures for LightNet Experiments** "Total batch size" means batch_per_gpu × update_freq × num_gpus; "ALM" stands for Autoregressive Language Model; "IM" stands for Image Modeling, "IG" stands for image generation.

	ALM	IM	IG
Dataset	WikiText-103	ImageNet-1k	ImageNet-1k
Tokenizer method	BPE	-	-
Src Vocab size	50265	-	-
Sequence length	512	-	-
Total batch size	128	2048	256
Number of updates/epochs	50k updates	300 epochs	80 epochs
Warmup steps/epochs	4k steps	20 epochs	-
Peak learning rate	5e-4	5e-4	1e-4
Learning rate scheduler	Inverse sqrt	Cosine	-
Optimizer	Adam	Adamw	Adamw
Adam ϵ	1e-8	1e-8	1e-8
Adam (β_1, β_2)	(0.9, 0.999)	(0.9, 0.98)	(0.9, 0.98)
Weight decay	0.1	0.1 for Base, else 0.05	0
Gradient clipping	-	5.0	-
GPUS	4	8	8

Table 12: **Configurations for LLM**

Params(B)	Layers	Hidden Dim	L.R.	Batch Size Per GPU	SeqLen	GPUs
1	18	2048	3.00E-04	10	2048	16
3	36	2560	3.00E-04	36	2048	48

Table 13: **Model Configurations for Image Generation task.**

Model	Layers	Hidden Dim	Heads	Params
LightNet-S	18	384	6	33M
LightNet-B	18	768	6	131M
LightNet-L	36	1024	16	470M
LightNet-XL	42	1152	16	680M

Table 14: **Model Configurations for Image Classification task.**

Model	Layers	Hidden size	Heads	Params
LightNet-T	12	192	6	6.0M
LightNet-S	12	384	16	22.6M
LightNet-B	12	768	16	87.7M